

Excited States of Crystalline Point Defects with Multireference Density Matrix Embedding Theory

Abhishek Mitra,^{†,||} Hung Q. Pham,^{‡,||} Riddhish Pandharkar,^{†,¶} Matthew R.
Hermes,[†] and Laura Gagliardi^{*,§,¶}

[†]*Department of Chemistry, Chicago Center for Theoretical Chemistry, University of
Chicago, Chicago, IL 60637, USA.*

[‡]*Department of Chemistry, Smith Hall, 207 Pleasant St SE, Minneapolis, MN 55455-0431,
USA*

[¶]*Argonne National Laboratory 9700 S. Cass Avenue Lemont, IL 60439*

[§]*Department of Chemistry, Pritzker School of Molecular Engineering, James Franck
Institute, Chicago Center for Theoretical Chemistry, University of Chicago, Chicago, IL
60637, USA.*

^{||}*Contributed equally to this work*

E-mail: lgagliardi@uchicago.edu

Abstract

Accurate and affordable methods to characterize the electronic structure of solids are important for targeted materials design. Embedding-based methods provide an appealing balance in the trade-off between cost and accuracy - particularly when studying localized phenomena. Here, we use the density matrix embedding theory (DMET) algorithm to study the electronic excitations in solid-state defects with a

restricted open-shell Hartree–Fock (ROHF) bath and multireference impurity solvers, specifically, complete active space self-consistent field (CASSCF) and n-electron valence state second-order perturbation theory (NEVPT2). We apply the method to investigate an oxygen vacancy (OV) on a MgO(100) surface and find absolute deviations within 0.05 eV between DMET using the CASSCF/NEVPT2 solver, denoted as CAS-DMET/NEVPT2-DMET, and the non-embedded CASSCF/NEVPT2 approach. Next, we establish the practicality of DMET by extending it to larger supercells for the OV defect and a neutral silicon vacancy in diamond where the use of non-embedded CASSCF/NEVPT2 is extremely expensive.

Quantum embedding theory offers an appealing solution for understanding the electronic structures of extended systems where conventional quantum chemical methods are impractical.¹ Various formulations of quantum embedding theory aims at describing a small region of interest, *i.e.*, a “fragment” or “impurity,” using an accurate yet expensive method while treating the rest of the system at a lower level of theory, usually a mean-field method such as Hartree–Fock (HF)² or Kohn-Sham density functional theory (KS-DFT).^{3,4} Density matrix embedding theory^{5–8} is a wave function-in-wave function embedding technique where the environment of the fragment is effectively modeled with a bath constructed by a Schmidt decomposition of a mean-field wave function.⁹ Recently, the DMET algorithm formulated using a restricted closed-shell Hartree–Fock (RHF) bath for solid-state systems within the framework of periodic boundary condition has been introduced independently by some of the authors¹⁰ as well as by Cui *et al.*¹¹ Our preliminary investigations revealed that DMET provides ground-state energies and band structures of simple solids like the periodic hydrogen chain and polyene.¹⁰

In this Letter, we investigate the performance of periodic DMET using the restricted open-shell Hartree–Fock (ROHF) wave function as a bath in describing open-shell excited states of point defects in solid-state systems. We implemented the complete-active space self-consistent field (CASSCF)^{12–14} and strongly-contracted n-electron valence state second-order

perturbation theory (NEVPT2)^{15–18} multireference methods as impurity solvers to capture electron correlation of excited states. While CASSCF has been used as a DMET solver within the molecular context,¹⁹ this is the first time that NEVPT2 is used as a high-level method in DMET. Our tests on the oxygen vacancy on a MgO(100) surface show that using ROHF as the low-level wave function in conjunction with the CASSCF/NEVPT2 solver offers an accurate description of strongly correlated electrons. The approach proposed here does not require the high-level wave function to break spin symmetry, as in the case in which the spin-unrestricted Hartree–Fock (UHF) method is employed for the low-level wave function.^{20,21} The theory and implementation of DMET for lattice models^{5,22,23} and molecular systems have been discussed extensively in previous publications. Readers are encouraged to refer to these publications for more details.^{7,8}

A spin-restricted Hartree–Fock wave function is used to initialize a periodic DMET calculation. The impurity is then defined using a set of localized orbitals in real space. We use the maximally-localized Wannier functions (MLWFs),^{24,25} implemented in the wannier90²⁶ code. The translational symmetry is broken for defective solids and the unit cell is chosen to be sufficiently large to avoid the interaction between periodic images of the defect. As a result, the Brillouin zone can be adequately sampled at the Γ -point and a subset of N_{imp} MLWFs at the chemical region of interest, for example those around the defective site, defines the impurity. The bath is a set of orbitals representing the environment and is constructed using the Schmidt decomposition,⁷ which for any single determinant requires only the one-body reduced density matrix (1-RDM). The environment block (D_{env}) of the 1-RDM is diagonalized, $D_{\text{env}} = \mathbf{U}\lambda\mathbf{U}^*$, where λ is a diagonal matrix of eigenvalues λ_i ($i = 1, 2, \dots, N_{\text{env}}$ where N_{env} is the number of the environment orbitals). The columns of the unitary matrix \mathbf{U} corresponding to λ_i other than zero or two define the entangled bath orbitals; the remainder are treated as a frozen core in the subsequent embedding calculation. For a RHF wave function, the number of $0 < \lambda_i < 2$ eigenvalues is at most N_{imp} . For a high-spin ROHF wave function, it is straightforward to prove that the number of $0 < \lambda_i < 2$ eigenvalues is at most $N_{\text{imp}} + 2S$,

where S is the total spin quantum number of the computational supercell. We thus denote DMET using the RHF and ROHF bath as DMET@RHF and DMET@ROHF, respectively. Following the Schmidt decomposition, the high-level wave function, $|\Psi_{\text{imp}}\rangle$, which formally diagonalizes the impurity Hamiltonian, \hat{H}_{imp} , in the combined Fock space of the impurity and bath orbitals can be determined by any high-level solver of choice, for instance, CASSCF or NEVPT2. All calculations are performed using our in-house pDMET code²⁷ and the PySCF package for electron integral and quantum chemical solvers.^{28,29} The calculations are all performed without enforcing any spatial symmetry. We will refer to the CASSCF or NEVPT2 calculations performed at the Γ -point without the use of DMET as non-embedding references or the full calculations. The computational methods used in this study are described in the Supporting Information (SI).

First, we consider the oxygen vacancy (OV) in magnesium oxide. This point defect plays a crucial role in energy storage and photoelectrochemical applications of metal oxides.³⁰⁻³² The oxygen vacancy exists both in the bulk as well as on the surface of the oxide. We investigate the performance of our method in calculating the first singlet-singlet and singlet-triplet excitations of a neutral oxygen vacancy, denoted here as OV, on the (100) monolayer of MgO. In particular, the removal of an oxygen atom (O) from the ionic crystal composed of the O^{2-} and Mg^{2+} ions results in two electrons trapped in the cavity left by the missing oxygen, denoted as a F-center (or a color center). The $\text{Mg}_{18}\text{O}_{18}$ model of OV is shown in Fig. 1a. The full space group of this monolayer model system contains the D_{4h} point group as a subgroup, and the two localized defect orbitals transform as the a_{1g} and a_{2u} irreducible representations, as shown in Fig. 1b (see Section S01 of the SI for more details on how the defect states are identified). Although the gaps between the valence band (VB) and conduction band (CB) obtained by RHF($S=0$) and ROHF($S=1$) are similar, the positions of the a_{1g} and a_{2u} orbitals with respect to the valence band maximum depend on the spin imposed in the mean-field calculation, as shown in Fig. 1c. Later, we extend our calculations to larger unit cells as shown in Fig. 1d. In the DMET calculations, we consider three impurity

clusters of expanding size to investigate how the choice of the impurity cluster affects the excitation energies (see Fig. 1e). The CASSCF and NEVPT2 methods are used as high-level solvers and the impurity is embedded in either the RHF or ROHF mean-field wave function. An active space of two electrons in two orbitals is employed in all calculations because there are two electrons and two defect orbitals localized at the F-center. The same active space was previously used.³³ We compare our embedding results with non-embedding Γ -point calculations on $\text{Mg}_{18}\text{O}_{18}$ at the same level of theory. The ground-state wave function for the F-center mainly consists of the $a_{1g}^{\uparrow\downarrow}$ determinant, leading to a ${}^1A_{1g}$ state. The first singlet excited-state, ${}^1A_{2u}$, results from the linear combination of the $a_{1g}^{\uparrow}a_{2u}^{\downarrow}$ and $a_{1g}^{\downarrow}a_{2u}^{\uparrow}$ determinants with an equal weight of *ca.* 48 %. Similarly, the first triplet excited-state, ${}^3A_{2u}$, is the $a_{1g}^{\uparrow}a_{2u}^{\uparrow}$ determinant.

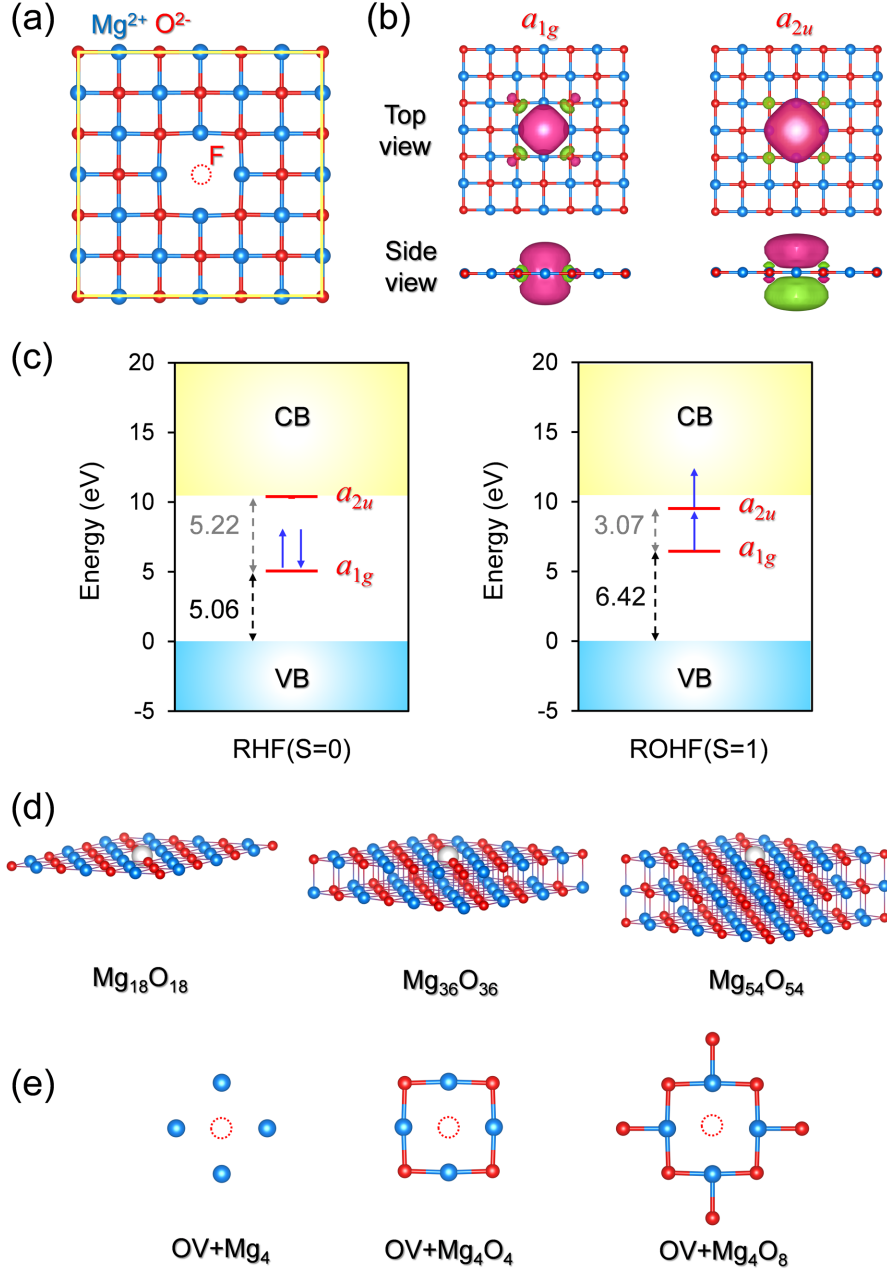


Figure 1: Oxygen vacancy on a $\text{Mg}_{18}\text{O}_{18}$ layer: (a) Top view of the F-center on the (100) surface. (b) Top and side view of two defect orbitals a_{1g} and a_{2u} from the $\text{ROHF}(S=1)$ calculation. The isosurface of orbitals is 0.03. (c) Relative energy of defect orbitals with respect to the valence band maximum. The Fermi energy (or valence band maximum) is set to 0; (d) Oxygen vacancy models with different numbers of layers: $\text{Mg}_{18}\text{O}_{18}$, $\text{Mg}_{36}\text{O}_{36}$, and $\text{Mg}_{54}\text{O}_{54}$. The top layer corresponds to (a) in each of these cases; The gray atom highlights the oxygen vacancy. (e) Three different impurity clusters considered in the DMET calculations. For $\text{Mg}_{36}\text{O}_{36}$ and $\text{Mg}_{54}\text{O}_{54}$, the Mg atom right below the vacancy is also included, resulting in $\text{OV}+\text{Mg}_5\text{O}_4$ instead of $\text{OV}+\text{Mg}_4\text{O}_8$.

Table 1: Vertical excitation energies (in eV) of the oxygen vacancy on the MgO(100) surface obtained using DMET with CASSCF and NEVPT2 as the solvers compared to CASSCF and NEVPT2 results at Γ -point. “Reference” here indicates the non-embedded Γ -point CASSCF and NEVPT2 calculations. The extrapolated CAS-DMET and NEVPT2-DMET energies from the linear regression are labeled as “Extrap”. All results are obtained using a (2,2) active space.

Excitation	Method	Impurity cluster	CASSCF	NEVPT2
${}^1A_{1g} \rightarrow {}^3A_{2u}$	DMET@RHF	OV+Mg ₄	2.70	3.22
		OV+Mg ₄ O ₄	1.78	2.53
		OV+Mg ₄ O ₈	1.37	2.18
		Extrap	1.10	1.98
	DMET@ROHF	OV+Mg ₄	1.30	1.91
		OV+Mg ₄ O ₄	1.32	2.09
		OV+Mg ₄ O ₈	1.32	2.12
		Extrap	1.33	2.18
	Reference		1.33	2.19
	${}^1A_{1g} \rightarrow {}^1A_{2u}$	DMET@RHF	OV+Mg ₄	5.38
OV+Mg ₄ O ₄			3.96	3.68
OV+Mg ₄ O ₈			3.30	3.05
Extrap			2.88	2.62
DMET@ROHF		OV+Mg ₄	3.27	3.17
		OV+Mg ₄ O ₄	3.26	3.05
		OV+Mg ₄ O ₈	3.25	3.00
		Extrap	3.25	2.97
Reference			3.25	2.95

Table 1 shows the vertical excitation energies for the OV system. The excitation energies are overestimated by DMET using the RHF($S=0$) bath. The deviation with respect to CASSCF for the largest impurity cluster OV+Mg₄O₈ is *ca.* 0.04 and 0.05 eV for the singlet-singlet and singlet-triplet excitation, respectively. For the ROHF($S=1$) bath, the smallest impurity cluster OV+Mg₄ already agrees well with CASSCF, with a deviation of 0.02-0.03 eV for both transitions. The excitation energies obtained using OV+Mg₄O₈ are almost identical to the CASSCF references. These results suggest that the bath constructed from a ROHF($S=1$) wave function is superior to that from the RHF($S=0$) wave function. Interestingly, we find a linear dependence between the NEVPT2 excitation energies and the inverse of the number

of embedding orbitals as shown in Figure 2, which suggests that it is realistic to extrapolate the NEVPT2-DMET energy to the one corresponding to the full system. It should be noted that similar convergence patterns have been observed and linear extrapolation techniques have been used in recent studies.^{34,35} Our extrapolations for the ROHF($S=1$) bath result in a deviation of only 0.02 and 0.01 eV for the singlet-singlet and singlet-triplet excitation, respectively between the embedding and non-embedding calculations. The same extrapolation for the RHF($S=0$) bath does not provide good agreement with the reference, highlighting the importance of a good DMET bath for both accuracy and efficiency for our embedding scheme.

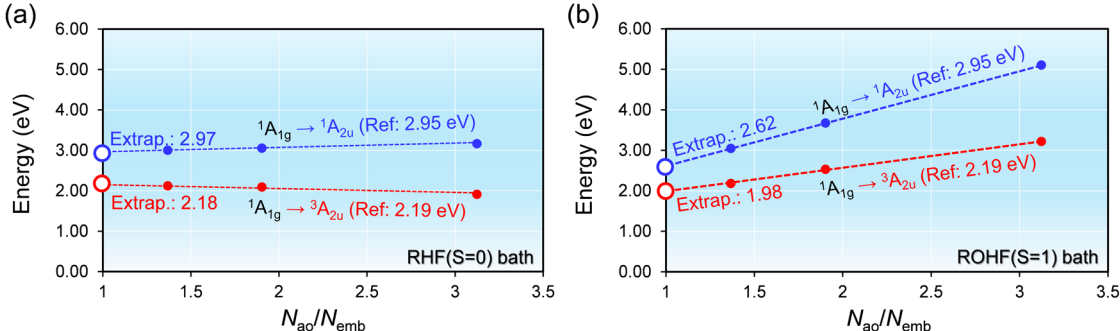


Figure 2: NEVPT2-DMET excitation energies of OV using (a) RHF($S=0$) bath and (b) ROHF($S=1$) bath as a function of N_{ao}/N_{emb} where N_{ao} is the number of basis functions of the entire system and N_{emb} is the number of embedding orbitals. The ${}^1A_{1g} \rightarrow {}^1A_{2u}$ and ${}^1A_{1g} \rightarrow {}^3A_{2u}$ transition are highlighted in blue and red, respectively. The extrapolated energy is indicated with the “Full” label. The reference NEVPT2 energy for each excitation is also given.

We extend our study to the oxygen vacancy on the MgO surfaces containing two or three layers, resulting in $Mg_{36}O_{36}$ and a $Mg_{54}O_{54}$ respectively (see Figure 1d). For these systems, we use a larger active space of two electrons in eight orbitals with s and p character localized at the defect (shown in the SI). The non-embedding CASSCF or NEVPT2 calculations for these models are not possible with our current computational capabilities. However, within the embedding framework, such calculations are possible. We investigate the performances of CAS-DMET and NEVPT2-DMET in calculating the singlet-singlet and singlet-triplet

excitation energies (shown in Table 2). The surface models with increasing number of layers allow us to study the convergence of the excitation energy with respect to the thickness of the slab. It is observed that although the $S_0 \rightarrow S_1$ excitation energies differ by 0.5-0.6 eV when moving from a single- to a double-layer model, the difference between the two- and three-layer models is about 0.1 eV for both $S_0 \rightarrow S_1$ and $S_0 \rightarrow T_1$ excitations. Moreover, the in-plane expansion of the layer model only slightly changes the excitation energies (see Section S05 of the SI). Unfortunately, there has yet been no consensus on the $S_0 \rightarrow S_1$ excitation energy of the surface F-center. The $S_0 \rightarrow S_1$ excitation is estimated to be about 1-5 eV by different experimental techniques.³⁶⁻³⁸ Computationally, the quantum mechanics/molecular mechanics (QM/MM) approach using the multireference configuration interaction (MRCI) method as the QM solver on a cluster model of OV predicts an excitation energy of 3.24 eV and 1.93 eV for the $S_0 \rightarrow S_1$ and $S_0 \rightarrow T_1$ excitations;³⁹ our CAS-DMET and NEVPT2-DMET calculations predict excitation energies 0.3-0.4 eV higher than this particular reference.

Table 2: Vertical excitation energies (in eV) of the oxygen vacancy on the MgO(100) surface obtained using CAS-DMET and NEVPT2-DMET using an (2,8) active space. The extrapolated CAS-DMET and NEVPT2-DMET energies from the linear regression are labeled as “Extrap”. The values preceded by a star correspond to the experimental measurement.

Excitation	Layers	Impurity cluster	CASSCF	NEVPT2	Literature
$S_0 \rightarrow T_1$	Mg ₁₈ O ₁₈	OV+Mg ₄	1.93	1.98	
		OV+Mg ₄ O ₄	1.97	2.07	
		OV+Mg ₄ O ₈	1.98	2.13	
		Extrap	1.99	2.11	
	Mg ₃₆ O ₃₆	OV+Mg ₄	2.19	2.19	
		OV+Mg ₄ O ₄	2.25	2.25	1.93 ³⁹
		OV+Mg ₄ O ₅	2.26	2.28	
		Extrap	2.32	2.35	
	Mg ₅₄ O ₅₄	OV+Mg ₄	2.20	2.13	
		OV+Mg ₄ O ₄	2.26	2.19	
		OV+Mg ₄ O ₅	2.28	2.21	
		Extrap	2.35	2.28	
$S_0 \rightarrow S_1$	Mg ₁₈ O ₁₈	OV+Mg ₄	3.48	3.37	
		OV+Mg ₄ O ₄	3.46	3.34	
		OV+Mg ₄ O ₈	3.45	3.30	
		Extrap	3.45	3.29	
	Mg ₃₆ O ₃₆	OV+Mg ₄	4.01	3.90	3.24 ³⁹
		OV+Mg ₄ O ₄	3.97	3.86	*2.30 ³⁶
		OV+Mg ₄ O ₅	3.91	3.75	*1.0, *1.3, *2.4, *3.4 ³⁷
		Extrap	3.87	3.70	*1.2, *3.6, *5.3 ³⁸
	Mg ₅₄ O ₅₄	OV+Mg ₄	3.90	3.79	
		OV+Mg ₄ O ₄	3.87	3.75	
		OV+Mg ₄ O ₅	3.81	3.67	
		Extrap	3.77	3.62	

Next, we discuss electronic excitations in the neutral silicon vacancy (SiV^0) in diamond, a typical qubit candidate and a bulk defective system.⁴⁰ In particular, we compute the first three singlet and first five triplet excitation energies, which have been studied previously using KS-DFT^{41–43} as well as density functional-based embedding techniques.^{44–46} The ground state of SiV^0 is a triplet, therefore, the use of a ROHF low-level wave function is necessary. Three models of increasing unit cell size representing the SiV^0 vacancy in diamond have been

explored as shown in Figure 3a. We considered two choices for the impurity cluster: SiC_6 and SiC_{12} as shown in Figure 3b. We report the excitation energies computed using the SiC_{12} impurity cluster in Table 3. The excitation energies computed using the smaller SiC_6 impurity cluster are reported in the SI. As one can expect, finite-size errors have a significant effect on the evaluation of excitation energies for both CAS-DMET and NEVPT2-DMET. The excitation energies differ by *ca.* 0.2-0.5 eV when moving from the SiC_{52} to the SiC_{126} unit cell, but only about 0.1 eV when moving from SiC_{126} to SiC_{214} . Additionally, we have used a finite cluster ($\text{SiC}_{54}\text{H}_{78}$) to compute excitation energies and have compared them with the periodic calculations. In Table 3, the excitation energies are compared with other computational and experimental values. Strictly speaking, the experimental number (1.31 eV) is a zero-phonon line (ZPL) and should not be directly compared to the vertical excitation energies. We are not aware of experimental data for the vertical excitation energy. The vertical excitation energies are expected to be larger depending on the excited state minimum. All our excitation energies are higher than those reported by Ma *et al.*^{44,45} We also note that Ma *et al.* used an active space of (16,9) and evaluated its convergence by adding only more doubly occupied orbitals. Here, we use a different active space of (10,12), which includes more unoccupied orbitals from the conduction band. The active orbitals (shown in the SI) are localized around the defect and have *s*-like, *p*-like and *d*-like characters from the silicon atom and the 6 surrounding carbon atoms which form the dangling SiC bonds. The singlet-triplet gaps for the SiC_{214} model are within 0.1 eV of the cluster calculations. The CASSCF and CAS-DMET triple-triplet excitations for SiC_{214} differ by 0.15-0.25 eV whereas the cluster NEVPT2 and NEVPT2-DMET differ by 0.3-0.5 eV.

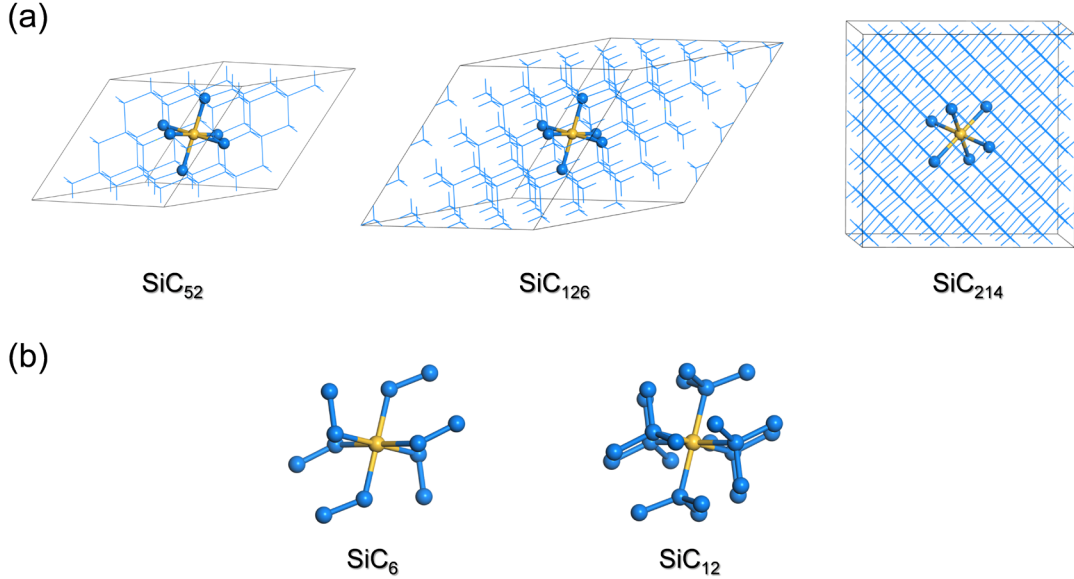


Figure 3: Neutral silicon vacancy in carbon diamond: (a) Three supercell models: SiC₅₂, SiC₁₂₆, and SiC₂₁₄. (b) The impurity clusters used in our DMET calculations: SiC₆ and SiC₁₂

Table 3: Singlet and triplet excitation energies (in eV) of SiV⁰ computed using CAS-DMET and NEVPT2-DMET using the SiC₁₂ impurity cluster shown in Figure 3b. The Table shows excitation energies for the SiC₅₂, SiC₁₂₆ and SiC₂₁₄ unit cells. The excitation energies reported under the “SiC₅₄H₇₈ cluster” column have been calculated using CASSCF and NEVPT2 calculations on a finite cluster SiC₅₄H₇₈. All calculations use an active space of (10,12). Computational values from literature are also included. The experimental value is the zero-phonon line and not a vertical excitation energy

State	CAS-DMET			NEVPT2-DMET			SiC ₅₄ H ₇₈ cluster		Literature	
	SiC ₅₂	SiC ₁₂₆	SiC ₂₁₄	SiC ₅₂	SiC ₁₂₆	SiC ₂₁₄	CASSCF	NEVPT2	Comput.	Expt.
T ₀	0.00	0.00	0.00	0.00	0.00	0.00	0.00	0.00		
T ₁	2.84	2.37	2.26	2.71	2.51	2.39	2.10	2.10	1.583 ⁴⁴	
T ₂	2.97	2.51	2.44	2.76	2.55	2.47	2.19	2.16	1.568, ⁴² 1.594 ⁴⁴	1.31 ⁴⁷
T ₃	3.03	2.54	2.44	2.85	2.55	2.46	2.25	2.14	1.568, ⁴² 1.594 ⁴⁴	1.31 ⁴⁷
T ₄	3.41	3.21	3.16	2.82	2.67	2.61	3.04	2.14	1.792 ⁴⁴	
S ₁	0.59	0.52	0.50	0.17	0.48	0.51	0.56	0.54	0.336 ⁴⁴	
S ₂	0.60	0.52	0.50	0.19	0.47	0.51	0.56	0.53	0.336 ⁴⁴	
S ₃	1.45	1.37	1.36	0.71	1.12	1.14	1.44	1.10	0.583 ⁴⁴	

Finally, we comment on the scaling of NEVPT2-DMET as compared to the reference NEVPT2 calculations. The computational cost of DMET is mainly dominated by the cost of the mul-

tireference calculations within the embedding space. The evaluation of the four-body reduced density matrix (4-RDM) required in NEVPT2 suffers from a scaling of $\mathcal{O}[N_{\text{det}} \times N_{\text{act}}^8]$, where N_{det} is the number of determinants (or configuration state functions, *i.e.*, CSF) and N_{act} is the number of active orbitals. NEVPT2-DMET has this step in common with NEVPT2. However, for a small number of determinants, the cost scaling in practical applications is controlled by the size of the parameter space, rather than the evaluation of the 4-RDM. The strongly contracted formalism¹⁸ employed throughout this work has an overall parameter space of $\mathcal{O}[N_{\text{det}} + N_{\text{inact}}^2 N_{\text{vir}}^2]$,⁴⁸ where N_{inact} and N_{vir} are the number of inactive (doubly occupied) and virtual (empty) orbitals, respectively. For, again, a small number of determinants, the computational cost of NEVPT2 will therefore exhibit an approximate scaling of $\mathcal{O}[N_{\text{inact}}^2 N_{\text{vir}}^2]$. NEVPT2-DMET removes unentangled orbitals from the parameter space, and therefore has a lower effective N_{inact} and/or N_{vir} than the corresponding NEVPT2 calculation. If all N_{core} unentangled orbitals are doubly occupied, the scaling of NEVPT2-DMET becomes $\mathcal{O}[(N_{\text{inact}} - N_{\text{core}})^2 N_{\text{vir}}^2]$; if they are all empty, the scaling of NEVPT2-DMET becomes $\mathcal{O}[N_{\text{inact}}^2 (N_{\text{vir}} - N_{\text{core}})^2]$. The advantage of the embedding treatment will become more significant for realistic applications using large basis set where the defect concentration is in fact very low. Therefore, the defect is often embedded in a large environment whose many unentangled orbitals can be excluded within the DMET framework.

In summary, we have generalized our periodic DMET to open-shell solids with the Brillouin zone sampled at the Γ -point in order to study the excited states of point defects. We have explored the performance of CASSCF and NEVPT2 as the high-level impurity solvers within the framework of density matrix embedding for solid-state systems. Our initial applications of the method demonstrate a good agreement between the embedding and the non-embedding calculations which are computationally expensive for the systems studied here. We have utilized DMET to compute CASSCF/NEVPT2 excitation energies in supercells where the non-embedding calculations become intractable. This paves the way for the applicability of multireference methods on a regular basis for periodic systems. We note that an algorithmic

improvement over the expensive computation of the exact exchange for periodic systems could further enhance the applicability of our method for large-scale computations of solid-state defects. Furthermore, the simple extension of the bath to open-shell solids introduced in this work can be generalized to the \mathbf{k} -point sampling of the Brillouin zone to study magnetic ordering in solids. We envision that the method proposed here will be used in the future to study quantum materials and extended systems containing lanthanides and actinides.

Associated content

Supporting Information. Computational details; A discussion on the better performance of the ROHF bath; Excitation energies for OV on a MgO(100) surface using a 2,2 active space; Total energies for supercells considered for OV in Mg(100) surface; Convergence of excitation energies in plane; Excitation energies using the SiC₆ impurity cluster in the silicon vacancy defect; Total energies for the cluster calculations for the silicon vacancy defect; Total Energies for supercells considered in the silicon vacancy defect; Active spaces explored within this work. This material is available free of charge via the Internet at <http://pubs.acs.org>.

Optimized crystal structures - cif files, Cluster geometries.

Associated content

Corresponding Author

*lgagliardi@uchicago.edu (L.G.)

Author Contributions

The manuscript was written through contributions of all authors. All authors have given approval to the final version of the manuscript.

Notes

The authors declare no competing financial interests.

Acknowledgement

We thank Giulia Galli, Joachim Sauer, Meagan Oakley and Debmalya Ray for insightful discussion. We are grateful to Zhihao Cui, Tianyu Zhu, Garnet K.-L. Chan for sharing with us the Gaussian density fitting transformation code. This work was funded by the Division of Chemical Sciences, Geosciences, and Biosciences, Office of Basic Energy Sciences of the U.S. Department of Energy through Grant DE-SC002183. Computer resources were provided by the Minnesota Supercomputing Institute at the University of Minnesota and the University of Chicago Research Computing Center.

References

- (1) Sun, Q.; Chan, G. K.-L. Quantum Embedding Theories. *Acc. Chem. Res.* **2016**, *49*, 2705–2712.
- (2) Szabo, A.; Ostlund, N. S. *Modern Quantum Chemistry: Introduction to Advanced Electronic Structure Theory*, 1st ed.; Dover Publications, Inc.: Mineola, 1996.
- (3) Hohenberg, P.; Kohn, W. Inhomogeneous Electron Gas. *Phys. Rev.* **1964**, *136*, B864–B871.
- (4) Kohn, W.; Sham, L. J. Self-Consistent Equations Including Exchange and Correlation Effects. *Phys. Rev.* **1965**, *140*, A1133–A1138.
- (5) Knizia, G.; Chan, G. K.-L. Density Matrix Embedding: A Simple Alternative to Dynamical Mean-Field Theory. *Phys. Rev. Lett.* **2012**, *109*, 186404.
- (6) Knizia, G.; Chan, G. K.-L. Density Matrix Embedding: A Strong-Coupling Quantum Embedding Theory. *J. Chem. Theory Comput.* **2013**, *9*, 1428–1432.
- (7) Wouters, S.; Jiménez-Hoyos, C. A.; Sun, Q.; Chan, G. K.-L. A Practical Guide to

- Density Matrix Embedding Theory in Quantum Chemistry. *J. Chem. Theory Comput.* **2016**, *12*, 2706–2719.
- (8) Wouters, S.; A. Jiménez-Hoyos, C.; K.L. Chan, G. *Fragmentation*; John Wiley & Sons, Ltd, 2017; Chapter 8, pp 227–243.
- (9) Peschel, I.; Eisler, V. Reduced Density Matrices and Entanglement Entropy in Free Lattice Models. *J. Phys. A* **2009**, *42*, 504003.
- (10) Pham, H. Q.; Hermes, M. R.; Gagliardi, L. Periodic Electronic Structure Calculations with The Density Matrix Embedding Theory. *J. Chem. Theory Comput.* **2020**, *16*, 130–140.
- (11) Cui, Z.-H.; Zhu, T.; Chan, G. K.-L. Efficient Implementation of Ab Initio Quantum Embedding in Periodic Systems: Density Matrix Embedding Theory. *J. Chem. Theory Comput.* **2020**, *16*, 119–129.
- (12) Roos, B. O.; Taylor, P. R.; Sigbahn, P. E. A Complete Active Space SCF Method (CASSCF) using A Density Matrix Formulated Super-CI Approach. *Chem. Phys.* **1980**, *48*, 157 – 173.
- (13) Siegbahn, P. E. M.; Almlöf, J.; Heiberg, A.; Roos, B. O. The Complete Active Space SCF (CASSCF) Method in A Newton–Raphson Formulation with Application to The HNO Molecule. *J. Chem. Phys.* **1981**, *74*, 2384–2396.
- (14) Siegbahn, P.; Heiberg, A.; Roos, B.; Levy, B. A Comparison of The Super-CI and The Newton-Raphson Scheme in The Complete Active Space SCF Method. *Phys. Scr.* **1980**, *21*, 323–327.
- (15) Angeli, C.; Cimiraglia, R.; Evangelisti, S.; Leininger, T.; Malrieu, J.-P. Introduction of n-electron Valence States for Multireference Perturbation Theory. *J. Chem. Phys.* **2001**, *114*, 10252–10264.

- (16) Angeli, C.; Borini, S.; Cestari, M.; Cimiraglia, R. A Quasidegenerate Formulation of The Second Order N-Electron Valence State Perturbation Theory Approach. *J. Chem. Phys.* **2004**, *121*, 4043–4049.
- (17) N-electron Valence State Perturbation Theory: A Fast Implementation of The Strongly Contracted Variant. *Chem. Phys. Lett* **2001**, *350*, 297 – 305.
- (18) Angeli, C.; Cimiraglia, R.; Malrieu, J.-P. N-electron Valence State Perturbation Theory: A Spinless Formulation and An Efficient Implementation of The Strongly Contracted and of The Partially Contracted Variants. *J. Chem. Phys.* **2002**, *117*, 9138–9153.
- (19) Pham, H. Q.; Bernales, V.; Gagliardi, L. Can Density Matrix Embedding Theory with The Complete Activate Space Self-Consistent Field Solver Describe Single and Double Bond Breaking in Molecular Systems? *J. Chem. Theory Comput.* **2018**, *14*, 1960–1968.
- (20) Bulik, I. W.; Scuseria, G. E.; Dukelsky, J. Density Matrix Embedding from Broken Symmetry Lattice Mean Fields. *Phys. Rev. B* **2014**, *89*, 035140.
- (21) Tran, H. K.; Ye, H.-Z.; Van Voorhis, T. Bootstrap Embedding with An Unrestricted Mean-field Bath. *J. Chem. Phys.* **2020**, *153*, 214101.
- (22) Zheng, B.-X.; Chan, G. K.-L. Ground-State Phase Diagram of The Square Lattice Hubbard Model from Density Matrix Embedding Theory. *Phys. Rev. B* **2016**, *93*, 035126.
- (23) Reinhard, T. E.; Mordovina, U.; Hubig, C.; Kretchmer, J. S.; Schollwöck, U.; Appel, H.; Sentef, M. A.; Rubio, A. Density-Matrix Embedding Theory Study of The One-Dimensional Hubbard-Holstein Model. *J. Chem. Theory Comput.* **2019**, *15*, 2221–2232.
- (24) Marzari, N.; Vanderbilt, D. Maximally Localized Generalized Wannier Functions for Composite Energy Bands. *Phys. Rev. B* **1997**, *56*, 12847–12865.

- (25) Marzari, N.; Mostofi, A. A.; Yates, J. R.; Souza, I.; Vanderbilt, D. Maximally Localized Wannier Functions: Theory and Applications. *Rev. Mod. Phys.* **2012**, *84*, 1419–1475.
- (26) Pizzi, G.; Vitale, V.; Arita, R.; Blügel, S.; Freimuth, F.; Géranton, G.; Gibertini, M.; Gresch, D.; Johnson, C.; Koretsune, T.; Ibañez-Azpiroz, J.; Lee, H.; Lihm, J.-M.; Marchand, D.; Marrazzo, A.; Mokrousov, Y.; Mustafa, J. I.; Nohara, Y.; Nomura, Y.; Paulatto, L.; Poncé, S.; Ponweiser, T.; Qiao, J.; Thöle, F.; Tsirkin, S. S.; Wierzbowska, M.; Marzari, N.; Vanderbilt, D.; Souza, I.; Mostofi, A. A.; Yates, J. R. Wannier90 as A Community Code: New Features and Applications. *J. Phys.: Condens. Matter* **2020**, *32*, 165902.
- (27) Pham, H. Q. pDMET: A Code for Periodic DMET Calculations. 2019; <https://github.com/hungpham2017/pDMET>, accessed Sep, 29, 2021.
- (28) Sun, Q.; Berkelbach, T. C.; Blunt, N. S.; Booth, G. H.; Guo, S.; Li, Z.; Liu, J.; McClain, J. D.; Sayfutyarova, E. R.; Sharma, S.; Wouters, S.; Chan, G. K.-L. PySCF: The Python-Based Simulations of Chemistry Framework. *Wiley Interdiscip. Rev. Comput.* **2018**, *8*, e1340.
- (29) Sun, Q.; Zhang, X.; Banerjee, S.; Bao, P.; Barbry, M.; Blunt, N. S.; Bogdanov, N. A.; Booth, G. H.; Chen, J.; Cui, Z.-H.; Eriksen, J. J.; Gao, Y.; Guo, S.; Hermann, J.; Hermes, M. R.; Koh, K.; Koval, P.; Lehtola, S.; Li, Z.; Liu, J.; Mardirossian, N.; McClain, J. D.; Motta, M.; Mussard, B.; Pham, H. Q.; Pulkin, A.; Purwanto, W.; Robinson, P. J.; Ronca, E.; Sayfutyarova, E. R.; Scheurer, M.; Schurkus, H. F.; Smith, J. E. T.; Sun, C.; Sun, S.-N.; Upadhyay, S.; Wagner, L. K.; Wang, X.; White, A.; Whitfield, J. D.; Williamson, M. J.; Wouters, S.; Yang, J.; Yu, J. M.; Zhu, T.; Berkelbach, T. C.; Sharma, S.; Sokolov, A. Y.; Chan, G. K.-L. Recent Developments in The PySCF Program Package. *J. Chem. Phys.* **2020**, *153*, 024109.

- (30) Wang, Z.; Wang, L. Role of Oxygen Vacancy in Metal Oxide Based Photoelectrochemical Water Splitting. *EcoMat* **2021**, *3*, e12075.
- (31) Sousa, C.; Tosoni, S.; Illas, F. Theoretical Approaches to Excited-State-Related Phenomena in Oxide Surfaces. *Chem. Rev.* **2013**, *113*, 4456–4495.
- (32) Richter, N. A.; Sicolo, S.; Levchenko, S. V.; Sauer, J.; Scheffler, M. Concentration of Vacancies at Metal-Oxide Surfaces: Case Study of MgO(100). *Phys. Rev. Lett.* **2013**, *111*, 045502.
- (33) Domínguez-Ariza, D.; Sousa, C.; Illas, F.; Ricci, D.; Pacchioni, G. Ground- and Excited-State Properties of M-center Oxygen Vacancy Aggregates in The Bulk and Surface of MgO. *Phys. Rev. B* **2003**, *68*, 054101.
- (34) Wang, X.; Berkelbach, T. C. Excitons in Solids from Periodic Equation-of-Motion Coupled-Cluster Theory. *J. Chem. Theory Comput.* **2020**, *16*, 3095–3103.
- (35) Gallo, A.; Hummel, F.; Irmeler, A.; Grüneis, A. A Periodic Equation-of-Motion Coupled-Cluster Implementation Applied to F-Centers in Alkaline Earth Oxides. *J. Chem. Phys.* **2021**, *154*, 64106.
- (36) Henrich, V. E.; Dresselhaus, G.; Zeiger, H. J. Energy-Dependent Electron-Energy-Loss Spectroscopy: Application to the Surface and Bulk Electronic Structure of MgO. *Phys. Rev. B* **1980**, *22*, 4764–4775.
- (37) Kramer, J.; Ernst, W.; Tegenkamp, C.; Pfnür, H. Mechanism and Kinetics of Color Center formation on Epitaxial Thin Films of MgO. *Surf. Sci.* **2002**, *517*, 87–97.
- (38) Wu, M.-C.; Truong, C. M.; Goodman, D. W. Electron-Energy-Loss-Spectroscopy Studies of Thermally Generated Defects in Pure and Lithium-Doped MgO(100) Films on Mo(100). *Phys. Rev. B* **1992**, *46*, 12688–12694.

- (39) Illas, F.; Pacchioni, G. Optical Properties of Surface and Bulk F Centers in MgO from Ab Initio Cluster Model Calculations. *J. Chem. Phys.* **1998**, *108*, 7835–7841.
- (40) Weber, J. R.; Koehl, W. F.; Varley, J. B.; Janotti, A.; Buckley, B. B.; Van de Walle, C. G.; Awschalom, D. D. Quantum Computing with Defects. *Proc. Natl. Acad. Sci. U.S.A.* **2010**, *107*, 8513–8518.
- (41) Gali, A.; Maze, J. R. *Ab initio* Study of The Split Silicon-Vacancy Defect in Diamond: Electronic Structure and Related Properties. *Phys. Rev. B* **2013**, *88*, 235205.
- (42) Thiering, G.; Gali, A. The $(e_g \otimes e_u) \otimes E_g$ Product Jahn–Teller Effect in The Neutral Group-IV Vacancy Quantum Bits in Diamond. *Npj Comput. Mater* **2019**, *5*, 18.
- (43) Ivády, V.; Abrikosov, I. A.; Gali, A. First Principles Calculation of Spin-related Quantities for Point Defect Qubit Research. *Npj Comput. Mater* **2018**, *4*, 76.
- (44) Ma, H.; Govoni, M.; Galli, G. Quantum Simulations of Materials on Near-Term Quantum Computers. *Npj Comput. Mater* **2020**, *6*, 85.
- (45) Ma, H.; Sheng, N.; Govoni, M.; Galli, G. First-Principles Studies of Strongly Correlated States in Defect Spin Qubits in Diamond. *Phys. Chem. Chem. Phys.* **2020**, *22*, 25522–25527.
- (46) Ma, H.; Sheng, N.; Govoni, M.; Galli, G. Quantum Embedding Theory for Strongly Correlated States in Materials. *J. Chem. Theory Comput.* **2021**, *17*, 2116–2125.
- (47) Green, B. L.; Doherty, M. W.; Nako, E.; Manson, N. B.; D’Haenens-Johansson, U. F. S.; Williams, S. D.; Twitchen, D. J.; Newton, M. E. Electronic Structure of The Neutral Silicon-Vacancy Center in Diamond. *Phys. Rev. B* **2019**, *99*, 161112.
- (48) Anderson, R. J.; Shiozaki, T.; Booth, G. H. Efficient and Stochastic Multireference Perturbation Theory for Large Active Spaces within A Full Configuration Interaction Quantum Monte Carlo Framework. *J. Chem. Phys.* **2020**, *152*, 054101.

Table of Contents graphic

